Analysis of an Autonomous Underwater Glider

Asher Bender, Daniel Matthew Steinberg, Ariell Lee Friedman, Stefan B. Williams
Australian Centre for Field Robotics
University of Sydney, Sydney, NSW 2006

Abstract

Underwater gliders have proven to be a powerful tool in oceanography because they are reusable, inexpensive and achieve a high duration. These qualities have made the acquisition of oceanographic data sets more accessible. The purpose of this article is to present a study aimed at modelling an underwater glider in the longitudinal and lateral plane. The proposed glider possesses a single stroke ballast pump, a moving internal mass and a symmetrical rudder design. It has an operational depth of 200m and is geared for coastal and estuarine environments. To provide the vehicle with navigation, a localisation algorithm capable of tracking an underwater glider and estimating ocean currents is proposed. The glider design is evaluated in simulation and results are presented illustrating the anticipated behaviour of this system.

1 Introduction

Understanding the oceans is not only scientifically relevant, it is also critical to human endeavours through its influence on climate, and as a provider of natural resources, recreation, tourism and fishing. Collecting sufficient and accurate data for marine-based research remains a pressing need given the domain's scale and harshness. Gliders operating in wider networks such as AOSN [AOSN, 2008] and IMOS [IMOS, 2008], are proving to be one of the most effective means of recording in-situ measurements of the water column on a spatial and temporal resolution that are necessary for understanding the oceans.

Underwater gliders are a class of autonomous submersibles approximately 2 metres in length which weigh around 50 kilograms and resemble sailplanes. Gliders are typically capable of extremely long missions (months to years), and may travel many thousands of kilometres in a single deployment.

Early oceanographers were only able to observe the depths of the ocean by deploying sensors from research ships. Although this method allows scientists to access the interior of the ocean, it is labour intensive, expensive and can only provide observations with a limited temporal and spatial density. Ship surveys are restricted in range and time by the needs of the crew and ship. As a result, typical ship surveys can only last a month or two [Davis et al., 2002]. This reliance on human intervention and ships created a need for autonomous oceanographic devices which could reduce the capital and labour cost of collecting data.

Floats and drifters represented the first great leap in autonomous oceanography. Drifters are floating devices which provide real-time oceanographic data as they drift with ocean currents. Floats also drift with ocean currents but cycle from the surface of the ocean to a pre-determined depth, taking measurements of temperature, salinity and depth as they drift [Gould, 2002]. These devices have been deployed in large numbers to allow ocean circulation models to be validated. Despite this, the location of their measurements are uncontrollable and, to a certain extent, unpredictable.

In 1989, Henry Stommel published a visionary article in Oceanography. Written from the perspective of an oceanographer in 2021, he envisioned the use of a fleet of "Slocums". He described them as floats that "migrate vertically through the ocean changing ballast, and they can be steered horizontally by gliding on wings" [Stommel, 1989]. In the following years, these devices became known as underwater gliders.

Gliders proved to be the next natural step in the development of autonomous oceanographic instruments. What distinguishes gliders from floats is that they are controllable. Oceanographers can determine where data will be collected by programming gliders to perform controlled 'flights' through the ocean.

Underwater gliders are useful for taking long-term, *in-situ* measurements of conditions within the water column. This application is particularly well suited to managing coastal resources and providing data which can be used to establish circulation and climate models. Multiple gliders can be deployed simultaneously in order to gather a wide range and high density of spatial and temporal data, and can be deployed relatively easily by two people in a small vessel [Davis et al., 2002].

The remainder of this paper is organized as follows: Section 2 presents more detailed background regarding modern day gliders and their use in oceanography; Section 3 focuses on modelling the equations of motion in the longitudinal plane for the case of an underwater glider with a single stroke ballast pump and a moving internal mass; Section 4 investigates the modelling and control of a glider in the lateral plane, as well as presenting an analysis of a glider's heading actuation system; Section 4 proposes a localisation algorithm capable of tracking an underwater glider and estimating ocean currents; and Section 6 provides concluding remarks and directions for future work.

2 Background

2.1 Modern Underwater Gliders

Currently, three notable underwater glider designs are widely used; Slocum [Webb et al., 2001], Spray [Sherman et al., 2001] and Seaglider [Eriksen et al., 2001].

Table 1 summarises the differences between the current glider designs. The information presented is summarised from [Davis et al., 2002] and [Rudnick et al., 2004].

Attribute	Slocum Electric	Spray	Seaglider
Hull (and Fairing)	1.5 m length, 21.3 cm diameter	2 m length, 20 cm diameter	1.8 m length, 30 cm diameter
Mass	52 kg	51 kg	52 kg
Batteries	260 alkaline C cells, 8 MJ	52 lithium CSC DD cells, 13 MJ	81 Lithium D cells, 10 MJ
Volume Change	520 cc, 90 W single stroke pump, 50% efficiency	900 cc, Motor & reciprocating pump, 20-50% efficiency	840 cc, Motor & reciprocating pump, 8-40% efficiency
Horiz Speed	0.4 m/s	0.45 m/s	0.45 m/s
Range	2300 km, 30 days @ 20° glide, 0.25 m/s horizontally	7000 km, 330 days, @ 18° glide, 0.25 m/s horizontally	4500 km, 220 days @ 18° glide, 0.25 m/s horizontally
Max Depth	200 m	1500 m	1000 m
Wings	98 cm span, 14 cm chord (MAC), 45° sweep	120 cm span, 10 cm chord (MAC)	100 cm span, 16 cm chord (MAC)

Table 1 - Glider Comparison

The gliders, Spray and Seaglider, are designed to operate at maximum depths from 1000 to 2000 metres. They have been optimised for minimal energy consumption and drag, and maximal range and mission duration. Conversely, the Slocum Electric is intended for shallow operation with a maximum depth of only 200 metres. Extended range is not the Slocum Electric's primary goal, but rather it has been optimised to be manoeuvrable for coastal and estuarine environments.

2.2 Operation

The physics behind underwater gliders is analogous to that of sailplanes. Wings on the glider create a lift force that acts perpendicular to its glide path and allows the glider to convert buoyancy into horizontal translation. This force is sufficient to overcome the drag force experienced by the vehicle and provides it with propulsion.

Gliders use buoyancy as their primary means of propulsion. The bulk of energy for gliding is supplied at the bottom of each dive cycle, where work is performed to increase the vehicle's volume to make it positively buoyant. At the apex of each dive cycle, the vehicle volume is decreased to make it negatively buoyant.

By concatenating a series of downwards and upwards glides, called yos, gliders can induce horizontal translation during their sawtooth glide (Figure 1).

Since drag is a quadratic function of velocity and gliders operate at relatively low speeds, they are more efficient than faster submersibles. However, this comes at the cost of lower speed and manoeuvrability. These factors allow for the long-range deployments seen with the current generation of underwater gliders [Graver, 2005].

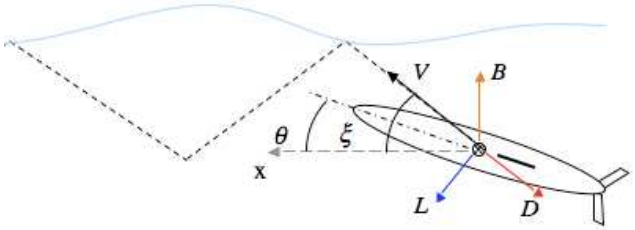

Figure 1 - The saw tooth glide path

2.3 Buoyancy Control

Buoyancy control is achieved by changing the vehicle's displaced volume. Different methods of controlling buoyancy in gliders exist. Reciprocating hydraulic pumps, as used in Spray and Seaglider, inflate and deflate a bladder with hydraulic oil to change the glider's buoyancy. These devices are small and light, but are relatively complicated to design. They have the added complexities of valves and plumbing, and are susceptible to more complex problems such as vapour lock when operating at high pressures. These mechanisms are most appropriately used for deep sea gliders [Geisbert, 2007].

Single-stroke piston pumps rely on gearing to obtain a high mechanical advantage to rotate a screw and extend or retract a piston in a cylinder. This approach is preferable for shallow-water operation, where rapid manoeuvrability and good two-way buoyancy control is important. This method is difficult to accomplish for deep sea, high-pressure, operation [Graver et al., 1998].

2.4 Pitch Control

Pitch, and consequently dive angle, is typically controlled by shifting an internal mass fore and aft within the glider. In most cases, this internal mass is made up of the batteries on a moveable sled. In some gliders, the primary pitching moment required between upward and downward glides may be achieved by locating the bladder or variable ballast at the nose of the glider. When the vehicle's buoyancy is changed, the relative change in the positions of the centre of buoyancy and the centre of gravity creates a moment that pitches the glider. Fine control of the pitch angle is then achieved by shifting the internal mass.

2.5 Heading Control

Two methods for controlling heading are currently used. The most intuitive means of changing heading is by deflecting a rudder to induce a yawing moment. A less intuitive method is to rotate an eccentric mass about the glider's longitudinal axis. This causes the glider to roll and allows a component of the lift force to act laterally; producing a spiral motion. Gliders that roll to turn achieve a turning radius of 20 to 30 m. Rudders are more suited to shallow operation and can induce a tighter turning circle of about 7m [Davis et al., 2002].

2.6 Localisation Methods Used in Modern Gliders

Several broad descriptions of how Slocum, Spray and Seaglider navigate are found in the 2001 series of articles published in the IEEE Journal of Oceanic Engineering [Webb et al., 2001; Sherman et al., 2001; Eriksen et al., 2001].

Slocum does not estimate water currents. To navigate, heading and glide angles are calculated between GPS fixes on the surface and are maintained during dives. The glider dead reckons whilst submerged using heading, vertical

velocity, pitch and buoyancy [Webb et al., 2001].

Like Slocum, Spray uses a simple navigation algorithm to compute the heading and dive angle required to reach a desired location from its current position. Spray neglects any currents and assumes a constant pitch, heading and angle of attack during its transit [Sherman et al., 2001]

Seaglider is unique in its ability to estimate water currents using a Kalman filter. Actual surface positions and those projected by dead reckoning during dive cycles are fused by the filter to estimate water currents [Eriksen et al., 2001]. Target heading and glide angle are adjusted to compensate for the estimated water currents. Compensation minimises power consumption and ensures that the vehicle approaches its target destination accurately.

The articles indicate that a GPS receiver, a depth sensor and a digital compass are available for navigation on all current gliders. However, it is clear from these articles that the majority of gliders do not compensate for water currents. Furthermore, only a scant description of how the gliders navigate has been provided in each article.

3 Buoyancy Engine and Pitch Control

This section focuses on a glider designed for operation in shallower coastal waters or estuaries with a maximum depth of 200 m. It employs a single stroke syringe type ballast pump located at the nose. Pitch is controlled by moving an internal battery mass fore and aft in the vehicle.

3.1 Glider Dynamics in the Longitudinal Plane

The following assumptions are used when modelling the buoyancy and pitch systems in the longitudinal plane:

1. The glider is designed symmetrically through its lateral and longitudinal body coordinate planes.
2. The mass moment of inertia of the vehicle about the y-axis is assumed to remain constant.
3. For the longitudinal model, the glider only travels in the vertical $x-z$ plane (Figure 2) with no yaw moment. As a result, hydrodynamic effects such as side force and induced rudder drag are neglected in the model.
4. The added mass of accelerating fluid during unsteady (non-equilibria) glider motion is assumed to be negligible. This is a simplifying assumption and a factor which should be kept in mind when basing any design decisions on the unsteady vehicle model

The positioning of ballast pump at the nose provides some of the nose-up/down moment required for ascent/decent. In texts such as [Graver, 2005], the glider's ballast system is modeled as a non-moving, variable point mass. This simplification omits the fact that the centroid of the buoyancy system moves. The centroid of the variable mass is dependent on the amount of fluid in the piston and on the moving, constant-mass assembly which pushes the piston back and forth. These factors were determined to have a significant impact on the pitching moment of the glider.

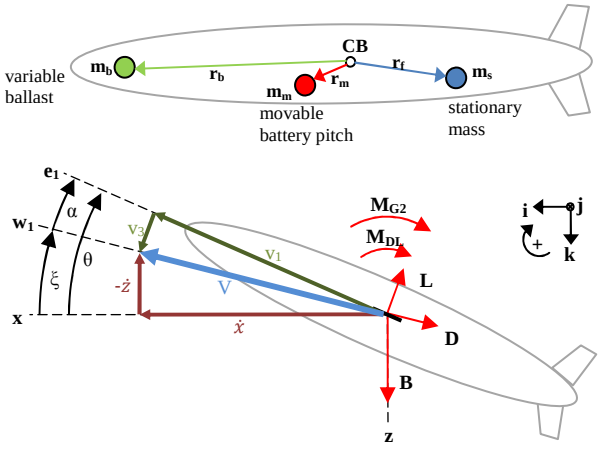

Figure 2 - Mass definitions, centroid locations and angles for longitudinal model

The following equations describe the dynamics of the glider in the longitudinal plane:

$$\ddot{x} = \frac{-\left(K_{D_o} + K_D\alpha^2\right)(\dot{x}^2+\dot{z}^2)\cos\xi - \left(K_{L_o} + K_L\alpha\right)(\dot{x}^2+\dot{z}^2)\sin\xi}{m_s + m_m + m_{b2} + \left(1-\frac{S_b}{L_p}\right)\forall_p\rho}$$

$$\ddot{z} = \frac{\left(K_{D_o} + K_D\alpha^2\right)(\dot{x}^2+\dot{z}^2)\sin\xi - \left(K_{L_o} + K_L\alpha\right)(\dot{x}^2+\dot{z}^2)\cos\xi - \frac{S_b}{L_p}\forall_p\rho g}{m_s + m_m + m_{b2} + \left(1-\frac{S_b}{L_p}\right)\forall_p\rho}$$

$$\begin{aligned}\ddot{\theta} = \frac{1}{J_2}\Big(&\left(K_{M_o} + K_M\alpha\right)(\dot{x}^2+\dot{z}^2) + K_{\Omega_2^1}\dot{\theta}\\ &-g\Big(\Big[m_s r_{s_i} + \left(1-\frac{S_b}{L_p}\right)\forall_p\rho\left(r_{p0_i} + \frac{S_b+L_p}{2}\right) + m_{b2}\left(r_{p0_i} + S_b - L_{b2}\right)\\ &+ m_m\left(r_{m0_i} + S_m\right)\Big]\cos\theta\\ &+\Big[m_s r_{s_k} + \left(\left(1-\frac{S_b}{L_p}\right)\forall_p\rho + m_{b2}\right)r_{p0_k} + m_m r_{m0_k}\Big]\sin\theta\Big)\Big)\end{aligned}$$

Where the K terms denote the constant hydro dynamic coefficients as per [Graver, 2005]. The angles α, ξ, θ represent the angle of attack, the glide-path angle and the pitch angle, respectively. The mass m_m, m_s terms are as outlined in Figure 2. In addition m_{b2} is the constant mass of the moving piston assembly and J_2 is the constant moment of inertia of the glider about the y-axis. r_{m0_i}, r_{p0_i} are the i^{th}components of the location to the movable mass and the piston under neutrally buoyant and zero pitch conditions. The piston parameters $L_p, \forall_p$ represent the piston's maximum stroke length and volume measured from the neutrally buoyant position. S_b and S_m are the positions of the piston and of the movable mass, respectively. ρ and g are the density of the fluid and the acceleration due to gravity.

Much of the glider's motion is actually in steady, un-accelerated gliding when the net forces and moments on the glider balance out to zero i.e., $\ddot{x}, \ddot{z}, \ddot{\theta} = 0$. In order to maintain a steady glide, the pitch angle must remain constant, so $\dot{\theta} = 0$. Equilibrium conditions are denoted by the subscript "eq".

Thus, for equilibrium:

$$0 = \frac{-\left(K_{D_o} + K_D\alpha_{eq}^2\right)V_{eq}^2\cos\xi_{eq} - \left(K_{L_o} + K_L\alpha_{eq}\right)V_{eq}^2\sin\xi_{eq}}{m_s + m_m + m_{b2} + \left(1-\frac{S_{b_{eq}}}{L_p}\right)\forall_p\rho}$$

$$0 = \frac{(K_{D_O} + K_D\alpha_{eq}^2)V_{eq}^2 \sin\xi_{eq} - (K_{L_O} + K_L\alpha_{eq})V_{eq}^2 \cos\xi_{eq} - \frac{S_{b_{eq}}}{L_p} \forall_p \rho g}{m_s + m_m + m_{b2} + \left(1 - \frac{S_{b_{eq}}}{L_p}\right) \forall_p \rho}$$

$$0 = \left((K_{M_O} + K_M\alpha_{eq})V_{eq}^2 - g\left(\left[m_s(r_{s_i}) + \left(1 - \frac{S_{b_{eq}}}{L_p}\right) \forall_p \rho \left(r_{p0_i} + \frac{S_{b_{eq}} + L_p}{2}\right)\right.\right.\right.$$
$$\left. + m_{b2}\left(r_{p0_i} + S_{b_{eq}} - L_{b2}\right) + m_m\left(r_{m0_i} + S_{m_{eq}}\right)\right]\cos\theta_{eq}$$
$$\left. + \left[m_s r_{s_k} + \left(\left(1 - \frac{S_{b_{eq}}}{L_p}\right) \forall_p \rho + m_{b2}\right) r_{p0_k} + m_m r_{m0_k}\right]\sin\theta_{eq}\right)\right)$$

We can also compute:

$$\theta_{eq} = \xi_{eg} + \alpha_{eq}$$

If values for ξ_{eq} and V_{eq} are nominated, the only unknowns in these equations are the angle of attack (α_{eq}), the pitch angle (θ_{eq}), the stroke position of the piston ($S_{b_{eq}}$) and the position of the movable mass ($S_{m_{eq}}$). There are now four equations and an equal number of unknowns.

Using the quadratic equation, it is possible to obtain the following solutions for α_{eq}:

$$\alpha_{eq} = \frac{1}{2K_D}\left(-K_L \tan\xi_{eq} \pm \sqrt{(K_L \tan\xi_{eq})^2 - 4(K_D)(K_{L_O}\tan\xi_{eq} + K_{D_O})}\right)$$

It should be noted that these solutions are only realisable if ξ_{eq} satisfies the discriminant condition, so if we restrict the values of the glide-path angle to be in the range $\xi_{eq} \epsilon \left\{-\frac{\pi}{2}, \frac{\pi}{2}\right\}$, it becomes apparent that the permissible glide-path angles are:

$$\tan^{-1}\left(\frac{2}{K_L^2}\left(K_D K_{L_O} + \sqrt{(K_D K_{L_O})^2 + K_L^2 K_D K_{D_O}}\right)\right) \leq \xi_{eq} \leq \frac{\pi}{2}$$

OR

$$-\frac{\pi}{2} \leq \xi_{eq} \leq \tan^{-1}\left(\frac{2}{K_L^2}\left(K_D K_{L_O} - \sqrt{(K_D K_{L_O})^2 + K_L^2 K_D K_{D_O}}\right)\right)$$

It is optimal to have a smaller angle of attack in terms of the hydrodynamics because it reduces drag-due-to-lift [Graver, 2005]. Therefore, the solution to equation for α_{eq} which yields less drag is chosen. During ascent when $\xi > 0$, the angle equilibrium angle of attack is:

$$\alpha_{eq} = \frac{1}{2K_D}\left(-K_L \tan\xi_{eq} + \sqrt{(K_L \tan\xi_{eq})^2 - 4(K_D)(K_{L_O}\tan\xi_{eq} + K_{D_O})}\right)$$

During descent when $\xi < 0$, the equilibrium angle of attack is:

$$\alpha_{eq} = \frac{1}{2K_D}\left(-K_L \tan\xi_{eq} - \sqrt{(K_L \tan\xi_{eq})^2 - 4(K_D)(K_{L_O}\tan\xi_{eq} + K_{D_O})}\right)$$

Now, the stroke position of the piston ($S_{b_{eq}}$) required for a steady state glide at a specified angle and speed can be solved:

$$S_{b_{eq}} = \frac{L_p V_{eq}^2}{\forall_p \rho g}\left((K_{D_O} + K_D\alpha_{eq}^2)\sin\xi_{eq} - (K_{L_O} + K_L\alpha_{eq})\cos\xi_{eq}\right)$$

The equilibrium position of the movable mass ($S_{m_{eq}}$) can be written as:

$$S_{m_{eq}} = \frac{1}{m_m}\left(\frac{V_{eq}^2}{g}(K_{M_O} + K_M\alpha_{eq})\sec\theta_{eq}\right.$$
$$- \left[m_s(r_{s_i}) + \left(1 - \frac{S_{b_{eq}}}{L_p}\right) \forall_p \rho \left(r_{p0_i} + \frac{S_{b_{eq}} + L_p}{2}\right)\right.$$
$$\left. + m_{b2}\left(r_{p0_i} + S_{b_{eq}} - L_{b2}\right) + m_m r_{m0_i}\right]$$
$$\left. - \left[m_s r_{s_k} + \left(\left(1 - \frac{S_{b_{eq}}}{L_p}\right) \forall_p \rho + m_{b2}\right) r_{p0_k} + m_m r_{m0_k}\right]\tan\theta_{eq}\right)$$

From the equations presented above, it is now possible to determine more specific operational requirements of the actuators based on the acceptable glide-path angles and velocities.

3.1 Simulation Results for the Longitudinal Plane

Figure 3 shows how the steady glide velocity varies with the equilibrium glide-path angle (ξ_{eq}) for several piston stroke positions, using the longitudinal glider model. Only upward glide angles are shown. For a symmetrical glider, downward glide speeds are the same as upward glide speeds.

It can be seen from Figure 3 that the horizontal velocity reaches a maximum at a specific glide-path angle of about 35°, irrespective of the piston position for this glider design. This result is useful as it implies that, given a constant piston stroke, a glide-path angle which maximises horizontal velocity can be nominated.

However, it should be pointed out that maximising the glider's horizontal velocity is not analogous to maximising the glider's horizontal range. The range of the glider is limited by its power capacity.

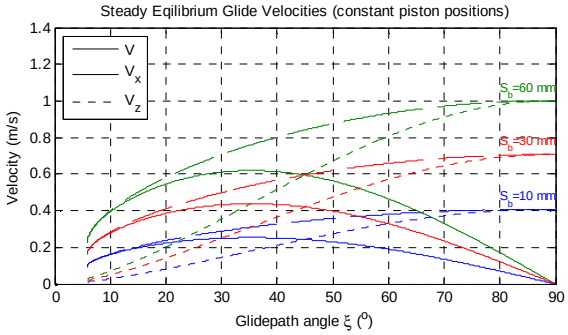

Figure 3 - Equilibrium glide velocities with selected piston stroke positions

During deep sea operation, the piston must do substantial work when pumping the ballast mass a small amount. At a steeper glide-path angle, the buoyancy actuator is required to operate at a higher frequency, increasing the average power required by the system. It is also possible to regulate the glide-path velocity so that the power consumed by the piston pump is constant over the range of glide-path angles. This is useful for practical operation of the glider as it provides a predictable endurance measurement based on a glider's design and energy specifications. Substituting the average power equation

$$P_{b_{av}} = \frac{V_{eq}\sin\xi_{eq}\rho g \forall_p S_{b_{eq}}}{L_p}$$

into the preceding equation for $S_{b_{eq}}$, it is possible to obtain the piston stroke position which is required for the constant power condition:

$$S_{b_{eq}} = \frac{L_p}{\forall_p \rho g}\left(\left(\frac{P_{b_{av}}}{\sin\xi_{eq}}\right)^2\left((K_{D_O} + K_D\alpha_{eq}^2)\sin\xi_{eq} - (K_{L_O} + K_L\alpha_{eq})\cos\xi_{eq}\right)\right)^{\frac{1}{3}}$$

Figure 4 shows how the glide velocity varies with respect to the glide-path angle for a few selected constant average power outputs of the piston.

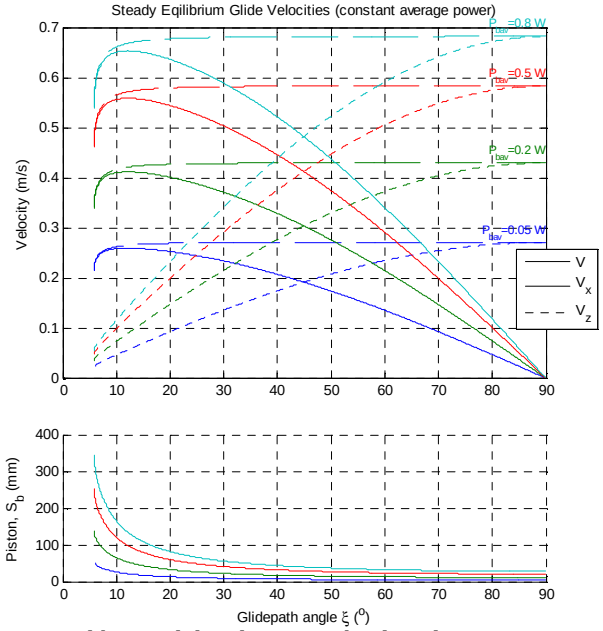

Figure 4 - Equilibrium glide velocities with selected piston power outputs

As a result, the choice of a steady glide-path angle should lie in the range $\hat{\xi} \in \{6°, 35°\}$. Glide-path angles steeper than 35° are achievable (depending on the actuation hardware), however it becomes inefficient in terms of reduced range and decreased horizontal velocity. The final choice is ultimately a trade-off between the speed of the glider, energy conservation and the desired density of oceanographic observations.

Glider speed is important in determining what environments the glider is capable of operating in. The expected currents during operation provide a design constraint for the glider's achievable speed. The glider should, at least, be able to overcome the average expected currents in the intended area of operation. The glider can be designed to go faster by adjusting the relative size of the piston ballast and using a low-drag hull design.

From these results, it is possible to design actuators capable of meeting the requirements for efficient operation.

4 Heading Control

Manoeuvrability is important for an underwater glider when operating in depths of less than 200 meters. Shallow mission gliders require a tight turning radius so that little altitude is sacrificed during turns. This increased manoeuvrability allows gliders to avoid obstacles. Hence a rudder is an appropriate choice for heading control.

In this section the effects of various non-linear, time variant aspects of a glider's design on the robustness of a linear PID controller are investigated. Furthermore, a brief investigation is made into energy efficient compensated transient response criteria of the control system. This will increase the deployable duration of the glider and aid in future control system design.

4.1 Glider Dynamics in the Lateral Plane

Before the rudder and heading control system can be designed and analysed, the dynamics that describe the motion of a glider in the lateral plane must be determined. For the purposes of this analysis the following simplifying assumptions were made for this section:

Assumption 1: Added mass and inertia contributions of the fluid surrounding the glider are initially assumed to be negligible.

Assumption 2: The sideslip angle, β, is assumed to be negligible in order to aid in decoupling the lateral equations of motion from the longitudinal plane. Hence all side forces and yawing moments due to sideslip are negligible.

Assumption 3: Rudder deflection does not induce any roll rate or angle since the rudder will be designed to be symmetrical about the centre of buoyancy (CB).

Using these assumptions, and the standard aerodynamic equations that describe the six degrees of freedom of a glider presented in [Graver, 2005] and [Geisbert, 2007], the following equations that describe side force, SF, and drag, D, experienced by the glider in the lateral plane (wind frame) were derived:

$$\begin{pmatrix} -D \\ SF \end{pmatrix} = \tfrac{1}{2}\rho S_{ref} V^2 \begin{pmatrix} -(C_{D0} + C_{DL}\alpha^2 + C_{DSF}\delta_r^2) \\ C_{SF\delta}\delta_r \end{pmatrix}$$

Here ρ is the density of sea water, S_{ref} is the wing planform area, V is the glider speed along its glide-path, δ_r is the rudder deflection angle, and C_{D0}, C_{DL}, C_{DSF}, $C_{SF\delta}$ are the coefficients of constant drag, drag-due-to-lift, drag-due-to-side force and the side force-curve slope of the rudder respectively.

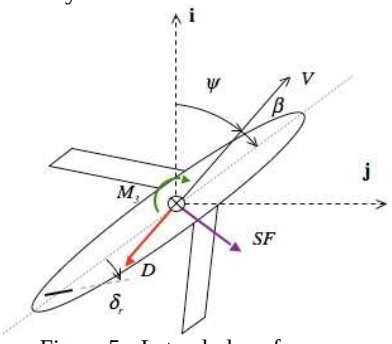

Figure 5 - Lateral plane forces

The hydrodynamic yaw moment was found to be:

$$M_3 = \tfrac{1}{4}\rho S_{ref}\bar{c}^2 V(C_{nr}\Omega_3) + \tfrac{1}{2}\rho S_{ref}\bar{c}V^2(C_{n\delta}\delta_r)$$
$$= \tfrac{1}{4}\rho S_{ref}\bar{c}^2 V(C_{nr}\Omega_3) + SF \cdot l_r$$

Where $\bar{c}$ is the mean aerodynamic chord, Ω_3 is the lateral angular velocity of the glider in the body frame, l_r, is the distance between the rudder aerodynamic centre and the glider CB, and C_{nr} and $C_{n\delta}$ are the yaw rate damping and yaw moment due to rudder deflection coefficients respectively. These forces are illustrated in Figure 5.

To study the controllability and efficiency of a glider, the following lateral plane equations of motion were derived using kinetics, $\Sigma M_3 = J_3\dot{\Omega}_3$, and Assumption 3, $\dot{\Omega}_3 = \ddot{\psi}\cos\theta$ –

$$\ddot{\psi} = \frac{\frac{1}{2}\rho V^2 S_{ref} C_{SF\delta} \delta_r \cdot l_r + \frac{1}{4}\rho V S_{ref} \bar{c}^2 C_{n_r} \dot{\psi} \cos\theta}{J_3 \cos\theta}$$

And from kinematics:

$$\begin{pmatrix} \dot{x} \\ \dot{y} \end{pmatrix} = \begin{pmatrix} V\cos\psi\cos\xi \\ V\sin\psi\cos\xi \end{pmatrix}$$

Here ψ is the glider heading and J_3 is the inertia of the glider in the lateral plane. These equations form the basis for the design of the rudder and heading control system.

By omitting angle of sideslip effects (Assumption 2), it is expected that the sum of moments presented in the glider equations of motion may be over- or under-stated. Furthermore, some lateral sideslip due to side force may be present in the actual glider's motion when changing heading, as mentioned in [Graver, 2005]. Similarly, it is expected that failing to account for added mass will lead to an overestimation of the system's natural transient response frequency. Precisely determining the added mass is beyond the scope of this study.

Despite these simplifying assumptions, a linear heading controller will be designed in the hope that further insights into the controllability of a glider will be provided. Furthermore, these simplified dynamics should still provide useful information about feasible rudder designs, and the energy consumption of the rudder actuator.

4.2 Heading Controller Robustness

This section summarizes a study of the robustness of a PID controller for use in controlling the glider's heading.

Firstly, the open-loop transfer function that describes heading as a function of rudder deflection needs to be found. Taking the Laplace transform of the kinetic heading equation:

$$\frac{\psi(s)}{\delta_r(s)} = \frac{2V^2(s) l_r C_{SF\delta} \sec\theta(s)}{\frac{4J_3}{\rho S_{ref}} s^2 - V(s)\bar{c}^2 C_{nr} s}$$

This is a second order time-variant system, which exhibits a very underdamped natural response. This is due to the fact that the poles of its closed-loop form have a very small magnitude, but stable, real component. It should be noted that including sideslip effects would make this transfer function non-homogenous which could potentially lead to an unstable natural response. Furthermore, the rudder actuator has a maximum deflection rate and the rudder lifting-surface will stall beyond a certain deflection angle. These have the effect of making the transfer function non-linear. A PID controller operates on the principles that the natural response of the system to be compensated is linear and time-invariant. Hence to facilitate controller design the glide-path velocity and pitch angle are assumed constant, and the system is assumed to be linear.

Using standard root locus methods [Nise, 2004], a controller can be designed based on desired transient response criteria, then tested for robustness by subjecting it to the non-linear and time-variant properties of the glider. Two controllers, designated controller 1 and controller 2, are designed in this manner. Controller 1 exhibits a settling time of 15 seconds and an overshoot of 20% ($K_D = 0.9152, K_P = 0.6156$). Controller 2 exhibits a settling time of 30 seconds and an overshoot of 5% ($K_D = 0.4353, K_P = 0.0672$). It should be noted that initially the effects of added mass/inertia are ignored as per Assumption 1.

Adding in the non-linear attributes of the rudder actuator and varying pitch while subjecting the system to a step heading change only marginally affects the compensated response of both controllers. However changing the glider's velocity and pitch, which occurs during an inflection, while subjecting the system to a step heading change noticeably increases the settling times and overshoots of both controllers, as can be seen in Figure 6. Controller 1 degrades the most in all test scenarios.

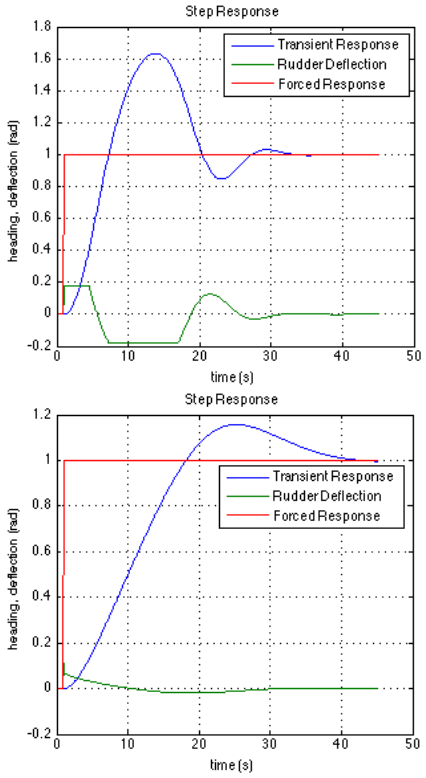

Figure 6 - Compensated transient response of controller 1 (top) and controller 2 (bottom) during an inflection.

The results suggest a PID controller is an appropriate control method, however longer settling times are more robust, and it would be wise to adjust the glider's heading during steady glides only. Furthermore, as an extension the effects of added mass were approximated. This rendered shorter settling times unachievable since the inertia of the system overcomes the rudder's ability to compensate. Hence longer settling times may be more appropriate when designing a controller.

4.3 Heading Transient Response Efficiency

Now that the robustness of the PID control method has been verified, reasonable compensated transient response criteria that enable energy efficient heading control can be found, while still providing adequate manoeuvrability.

The power required to rotate the glider's rudder was estimated as follows:

$$P_{input} = \frac{1}{\eta} K_S |\delta_r| \cdot |\dot{\delta}_r|$$

Where η is the efficiency of the actuator, and K_S is the spring coefficient of the seal (2.29 Nm/rad). The energy required to change heading is simply the integral of the power equation:

$$E_{input} = \int P_{input} \cdot dt$$

In order to determine desirable compensated transient responses, a scenario was simulated in which the glider travelling at 0.4m/s along a glide path of ±20° has to make a 90° heading change after 1 second. It is essential that the controller can manoeuvre the glider within the range of a detected obstruction, which is taken to be approximately 20 m.

The following table is a summary of the compensated transient responses tested – where the manoeuvring distance is the distance taken to execute the heading change along the glider's original heading:

Settling Time	Overshoot (%)	Energy Consumed (J)	Manoeuvring Distance (M)
15	20	0.897	1.99
15	1	0.474	2.89
30	1	0.097	5.27
45	1	0.073	7.72

Table 2 - Results of energy consumption and manoeuvring test

As can be seen from Table 2, large overshoot in a transient response is undesirable because it leads to large rudder adjustments which consume a significant amount of energy. Transient responses with settling times greater than about 45 seconds only consume marginally less energy than 30-40 second settling times, however the manoeuvring distance still shows a distinct increase (Figure 7) – which may not be worth the marginal energy savings.

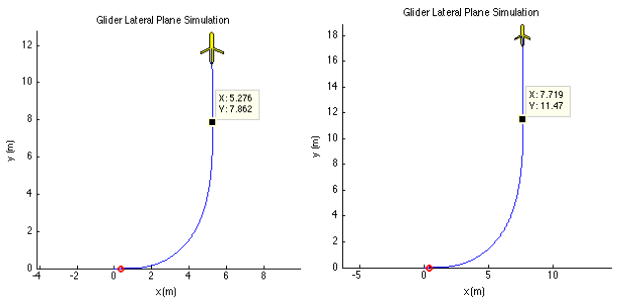

Figure 7 - Manoeuvring distances, as given by the *x* distance, for the 30 second (left) and 45 second (right) transient response tests

Furthermore, it was found that the exact amount of energy consumed when controlling heading is a function of rudder design. The greater the side force-curve slope of the rudder, $C_{SF\delta}$, the less the rudder will have to be deflected to generate the same force, hence requiring less energy. However drag-due-to-side force is a function of the side force-curve slope, as demonstrated in the following equation:

$$C_{DSF} = \frac{C_{SF\delta}^2}{\pi A_r e} \cdot \frac{S_r}{S_{ref}}$$

Where A_r is the aspect ratio of the rudder, e is the efficiency of the rudder, and S_r is the rudder planform area. Similarly, while a larger rudder area will increase its side force per deflection angle, it will also contribute more to the pressure and skin drag of the glider (C_{D0}). Hence a trade-off is encountered in the design of the rudder between maximising the efficiency of heading control, and of drag contribution to the glider. Conversely, manoeuvring distance exhibits a kinematic relationship with the chosen transient response and will be similar for all rudder designs which can overcome the total inertia of the glider to achieve the desired transient response.

5 Underwater Glider Localisation

Although gliders have provided oceanographers with a convenient method for collecting high resolution data, the majority of underwater gliders are unable to estimate ocean currents in real time [Webb et al., 2001; Sherman et al., 2001]. This weakness places a limit on the spatial accuracy of the oceanographic data sets produced by these gliders.

Real time estimation of water currents will allow gliders to more accurately locate where oceanographic data were sampled and permit higher level planning modules to synthesise routes which minimise navigational errors created by water currents. In turn, this will reduce energy spent on course corrections and allow gliders to increase their endurance. Estimating the location of underwater gliders is a challenge as they:

- have a small set of sensors available to describe their environment
- operate for extended periods without direct measurements of their location
- have limited power and memory resources

5.1 Localisation Algorithm Design

Localisation of autonomous underwater vehicles has been extensively studied in the literature [Roman, 2005; Williams and Mahon, 2004; Yun et al. 2000]. Drawing inspiration from these techniques, it can be shown that more accurate localisation of underwater gliders can be achieved using the limited navigational sensors available on underwater gliders.

Vehicle Model

From a mechanical design point of view, it is necessary to understand what forces will act on the vehicle. However, localisation is generally only concerned with position and motion. The relatively slow motion of the glider suggests that kinematic models may be sufficient to capture the motion of the vehicle.

Only velocity (v), roll (ϕ), pitch (θ) and yaw (ψ) are necessary to describe the change in vehicle displacement over a small time period (Δt) as show in Figure 8.

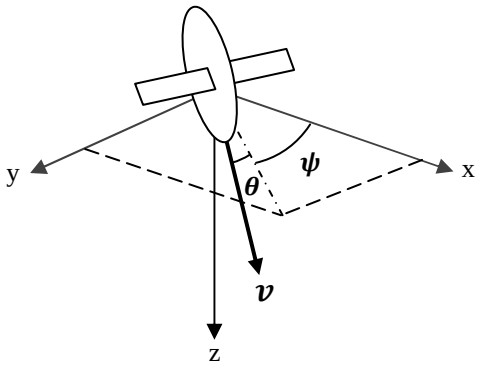

Figure 8 - Geometry of Vehicle Trajectory

Water Current Model

To allow the localisation filter to estimate water currents, a model must be established to represent the hidden forces resulting from them. The assumptions used to model water currents are adopted from [Graver, 2005]. These are:

- Water currents will be modelled in the world frame
- Gliding motions with water currents can be modelled as the superposition of water current velocities onto gliding motions without water currents

Water currents can be broken down into an easting (ε) current which represents the x component of water velocity and a northing current (η) which represents the y component, as shown in Figure 9.

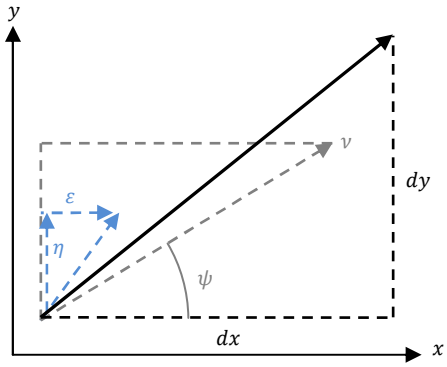

Figure 9 - Water Current Model in XY plane

The displacement due to the water current is shown in light blue. The displacement due to gliding motion without water currents are shown in gray. The superposition of these displacements is shown in black.

Dead Reckoning Model

If the geometry from Figure 8 and Figure 9 is utilised, the following discrete dead reckoning equations can be composed:

$$x_n = x_0 + \sum_{i=0}^{n-1} v_i \Delta t_i \cos\theta_i \cos\psi_i + \Delta t_i \varepsilon_i$$

$$y_n = y_0 + \sum_{i=0}^{n-1} v_i \Delta t_i \cos\theta_i \sin\psi_i + \Delta t_i \eta_i$$

$$z_n = z_0 + \sum_{i=0}^{n-1} v_i \Delta t_i \sin\theta_i$$

Since the estimate of vehicle pose at time n relies on the prior estimate at time $n-1$ and a noisy vehicle model, the uncertainty in the estimated state will grow without bound using dead reckoning alone. Absolute position observations, such as those provided by a GPS when the vehicle is on the surface, can help to bound this growth in uncertainty.

Fortunately, these equations can be represented in state-space and implemented in an Extended Kalman Filter (EKF) [Gelb, 1974]. Using an EKF as a navigational filter is an ideal way to manage system model error and fuse data from sensors into the system.

Correlation between states allows the EKF to produce estimates of unobserved processes. Two processes on the glider are unobservable and will be estimated by the filter: the glider's velocity and the effect of water currents.

Establishing an Extended Kalman Filter

Using state-space notation, the process state can be defined using the variables presented in Figure 8 and Figure 9:

$$\boldsymbol{x} = [x \quad y \quad z \quad \phi \quad \theta \quad \psi \quad v \quad \varepsilon \quad \eta]^T$$

To propagate the state, the dead reckoning equations can be written in vector notation to compose the state transition model and stated in a way that is consistent with the EKF equations:

$$\boldsymbol{f}(\boldsymbol{x}, t) = \begin{bmatrix} x + v\Delta t \cos\theta \cos\psi + \Delta t\varepsilon \\ y + v\Delta t \cos\theta \sin\psi + \Delta t\eta \\ z + v\Delta t \sin\theta \\ \phi \\ \theta \\ \psi \\ v \\ \varepsilon \\ \eta \end{bmatrix} + \begin{bmatrix} w_x \\ w_y \\ w_z \\ w_\phi \\ w_\theta \\ w_\psi \\ w_v \\ w_\varepsilon \\ w_\eta \end{bmatrix}$$

These equations assume that linear and angular velocities are constant over the observed time period (Δt). Under this assumption, accelerations are considered to be nonexistent or negligible between samples and can be omitted from the model. This simplifies the model greatly by reducing the number of variables in the system.

For the proposed localisation algorithm, sources of error will be considered uncorrelated and the disturbance matrix will be defined as:

$$\boldsymbol{Q} = \text{diag}\left(\left[\sigma_x^2 \quad \sigma_y^2 \quad \sigma_z^2 \quad \sigma_\phi^2 \quad \sigma_\theta^2 \quad \sigma_\psi^2 \quad \sigma_v^2 \quad \sigma_\varepsilon^2 \quad \sigma_\eta^2\right]\right)$$

Conveniently, all the sensors typically employed on gliders are absolute sensors and present their data in the inertial frame. These include GPS for position, pressure sensors for depth, and attitude heading reference sensors for heading, roll and pitch. This simplifies the measurement models as no transformations are required to fuse the data with the estimate. To allow asynchronous measurement, individual measurement models and their respective uncertainty models are created for each sensor:

$$\nabla H_{GPS} = \begin{bmatrix} 1 & 0 & 0 & 0 & 0 & 0 & 0 & 0 & 0 \\ 0 & 1 & 0 & 0 & 0 & 0 & 0 & 0 & 0 \end{bmatrix} \qquad R_{GPS} = \begin{bmatrix} {\sigma_X}^2 & 0 \\ 0 & {\sigma_Y}^2 \end{bmatrix}$$

$$\nabla H_{Depth} = [0 \quad 0 \quad 1 \quad 0 \quad 0 \quad 0 \quad 0 \quad 0 \quad 0] \qquad R_{Depth} = {\sigma_Z}^2$$

$$\nabla H_{AHRS} = \begin{bmatrix} 0 & 0 & 0 & 1 & 0 & 0 & 0 & 0 & 0 \\ 0 & 0 & 0 & 0 & 1 & 0 & 0 & 0 & 0 \\ 0 & 0 & 0 & 0 & 0 & 1 & 0 & 0 & 0 \end{bmatrix} \qquad R_{AHRS} = \begin{bmatrix} {\sigma_\phi}^2 & 0 & 0 \\ 0 & {\sigma_\theta}^2 & 0 \\ 0 & 0 & {\sigma_\psi}^2 \end{bmatrix}$$

The localisation algorithm will assume all bias and scale factors have been calibrated out of the sensors and that all sources of error are uncorrelated. This assumption allows measurements to be fused asynchronously.

5.2 Results of Testing Localisation Algorithm

A kinematic model of an underwater glider was developed to test the proposed algorithm. Testing revealed that the localisation algorithm is able to track the glider accurately in the presence of water currents over a range of conditions (Figure 10).

The tests performed were relatively simple simulations of real world processes. The biggest weakness in the testing process was the method used to generate glider data. Since a simple kinematic model of the glider was used to generate trajectory data, the localisation algorithm is highly representative of the input process. This accuracy inflates the overall success of the localisation algorithm.

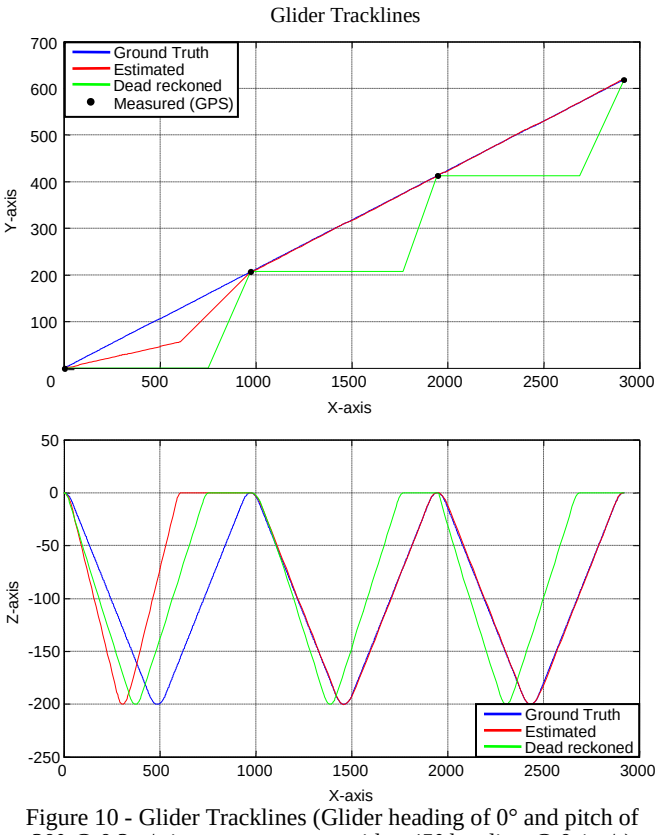

Figure 10 - Glider Tracklines (Glider heading of 0° and pitch of 30° @ 0.3m/s in a water current with a 45° heading @ 0.1m/s)

A more thorough method for testing the filter would be to run the localisation algorithm on the output of a more accurate dynamic glider simulation. Alternatively, testing the proposed algorithm on real data, collected by gliders operating in the field, would serve to validate the proposed approach. This would help determine whether a kinematic localisation algorithm is able to properly track glider motion.

Despite simplifications in the testing process, the localisation algorithm proves several important points:

1. A Kalman filter is able to resolve water currents by exploiting the difference between dead reckoned positions and GPS positions
2. A GPS receiver, a depth sensor and a digital compass are sufficient sources of external data for localisation and estimation of water currents when the system process model closely matches the real world process

Even if the kinematic assumption used does not prove to be valid in more realistic scenarios, a sufficiently detailed dynamic system model ought to produce accurate localisation.

Recommendations for future work include more rigorous experimental validation of the localisation algorithms. The localisation algorithm presented ignores the effect of control input. Localisation can be improved by including the effects of actuation in the system process model. Unless the effects of actuation are over simplified, they can only really be described by resorting to a dynamic representation of the process model. Adopting a dynamic model would allow the internal states of the system to be included in the system process model such as the location of the pitch mass and the amount of buoyancy provided by the buoyancy engine.

6 Conclusion

The body of work contained in this paper presents research carried out on three interesting aspects of underwater gliders. Underwater glider models are presented for both the lateral and longitudinal plane. These models are used to validate hardware designs capable of providing an underwater glider with buoyancy, pitch and heading control. To enhance navigation, an EKF capable of tracking an underwater glider and estimating ocean currents is proposed.

Future work will include unification of the longitudinal model presented in Section 3 and the lateral plane model presented in Section 4 to fully incorporate the six-degrees of freedom of the glider's dynamics. This model could provide further insight into the controllability, stability and performance of gliders. The complete dynamic system model could also be used to include the effect of control input in the localisation algorithm which may improve location estimates.

The abilities of underwater gliders can be extended by adopting technologies used in larger AUVS. A motorised hybrid glider would possess a unique mixture of qualities. The hybrid vehicle would conserve energy by employing conventional glider behaviour to reach target destinations. Unlike conventional gliders it would be capable of level flight at these destinations which would permit the use of sensing payloads such as those used for benthic surveying.

These vehicles hold much promise, particularly the potential to revolutionise the way oceanographic surveys are executed. An AUV capable of long range missions could be launched and recovered from the coast or in sheltered coastal bays. This convenience would eliminate the need for a dedicated and costly support ship during deployment and recovery. Eliminating the need for support ships will reduce the cost of benthic surveys, minimise human intervention and reduce in-water risk.

7 References

[AOSN, 2008] Autonomous Ocean Sampling Network, Accessed 20/10/2008 from: http://www.mbari.org/aosn/

[Brown, 1992] R. G. Brown and P. Y. C. Hwang, Introduction to Random Signals and Applied Kalman Filtering, Second ed. New York: Wiley, 1992.

[Davis et al., 2002] R. E. Davis, C. C. Eriksen, and C. P. Jones, "Autonomous Buoyancy-driven Underwater Gliders," The Technology and Applications of Autonomous Underwater Vehicles, 2002.

[Eriksen et al., 2001] C. C. Eriksen, T. J. Osse, R. D. Light, T. Wen, T. W. Lehman, P. L. Sabin, J. W. Ballard, and A. M. Chiodi. Seaglider: a long-range autonomous underwater vehicle for oceanographic research. Oceanic Engineering, IEEE Journal of, vol. 26, pp. 424-436, 2001.

[Geisbert, 2007] J. S. Geisbert, "Hydrodynamic Modeling for Autonomous Underwater Vehicles Using Computational and Semi-Empirical Methods," Masters, Virginia Polytech Institute and State University, Blacksburg, 2007.

[Gelb, 1974] A. Gelb. Applied Optimal Estimation. Cambridge, Massachusetts, and London, England: The M.I.T. Press, 1974.

[Gould, 2002] W. J. Gould, "A Brief History of Float Developments," South Hampton Oceanography Centre, 2002, Accessed 20/10/2008 from http://www.noc.soton.ac.uk/JRD/HYDRO/argo/history.php

[Graver, 2005] J. G. Graver. Underwater Gliders: Dynamics, Control and Design. PhD: Princeton University, 2005.

[Graver et al., 2002] J. G. Graver, J. Liu, C. Woolsey et al., "Design and Analysis of an Underwater Vehicle for Controlled Gliding," in Conference on Information Sciences and Systems (CISS), Princeton, 1998.

[IMOS, 2008] Integrated Marine Observing System Accessed 20/10/2008 from: http://imos.org.au/home.html

[Nise , 2004] N. S. Nise, Control Systems Engineering, Fourth ed., Hoboken, NJ: John Wiley & Sons, Inc., 2004.

[Roman, 2005] Roman, C. N. Self Consistent Bathymetric Mapping from Robotic Vehicles in the Deep Ocean. PhD: MIT - WHOI Joint Program, 2005.

[Rudnick et al., 2004] D. L. Rudnick, R. E. Davis, C. C. Eriksen et al., "Underwater Gliders for Ocean Research," Marine Technology Society Journal, vol. 38, no. 1, Spring, 2004.

[Stommel, 1989] H. Stommel The Slocum Mission. Oceanography, pp. 22 - 25, April 1989.

[Sherman et al., 2001] J. Sherman, R. E. Davis, W. B. Owens, and J. Valdes. The autonomous underwater glider "Spray". Oceanic Engineering, IEEE Journal of, vol. 26, pp. 437-446, 2001.

[Webb et al., 2001] D. C. Webb, P. J. Simonetti, and C. P. Jones. SLOCUM: an underwater glider propelled by environmental energy. Oceanic Engineering, IEEE Journal of, vol. 26, pp. 447-452, 2001.

[Williams and Mahon, 2004] Williams, S. and I. Mahon. Simultaneous localisation and mapping on the Great Barrier Reef. In: Proc. IEEE Intl. Conf. Robot. Auto.. Vol. 2. pp. 1771–1776, 2004.

[Yun et al. 2000] Yun, X., E. Bachmann, S. Arslan, K. Akyol and R. McGhee. An inertial navigation system for small autonomous underwater vehicles. In: Proc. IEEE Intl. Conf. Robot. Auto.. Vol. 2. San Francisco, CA. pp. 1781–1786, 2000.